Hydrogen Partitioning into Molten Iron at High Pressure: Implications for Earth's Core

Takuo Okuchi

Because of dissolution of lighter elements such as sulfur, carbon, hydrogen, and oxygen, Earth's outer core is about 10 percent less dense than molten iron at the relevant pressure and temperature conditions. To determine whether hydrogen can account for a major part of the density deficit and is therefore an important constituent in the molten iron outer core, the hydrogen concentration in molten iron was measured at 7.5 gigapascals. From these measurements, the metal-silicate melt partitioning coefficient of hydrogen was determined as a function of temperature. If the magma ocean of primordial Earth was hydrous, more than 95 mole percent of H_2O in this ocean should have reacted with iron to form FeH*x*, and about 60 percent of the density deficit is reconciled by adding hydrogen to the core.

To simulate metal-silicate melt partitioning of H in the early history of Earth, I synthesized iron hydride (FeH*x*) in an ultrabasic hydrous silicate melt. Experiments were conducted at 7.5 GPa with a uniaxial, multianvil apparatus (*1*). Starting materials (Table 1) were prepared from mixtures of iron, MgO, brucite [$Mg(OH)_2$], silica glass (SiO_2), silicic acid ($SiO_2 \cdot 0.4H_2O$), and liquid H_2O and were sealed in Pt capsules that were 5 mm in outside diameter, 0.2 mm thick, and 7 mm long. These large capsules can enclose a maximum of 20 mg of H_2O with the iron and silicate components, and this amount of H_2O was required to buffer hydrogen pressure (p_{H_2}) throughout the experiments (*2*). Temperature variations within these capsules were reduced to less than 100°C by thermal insulation (*3*).

The melting temperature of Fe is reduced by addition of H (*4–6*). At 7.5 GPa the melting temperature of FeH*x* lies between 1100°C and 1200°C (*3*), which is 600°C lower than that of Fe. When FeH*x* melts in a molten silicate, it segregates, forms large droplets (*4, 7*), and rapidly settles to the base of the capsule because FeH*x* melt is immiscible in a silicate melt. The experiments should be finished before all the droplets settle; for this reason the duration of each experiment was limited (Table 1). This duration may appear too short but the equilibrium was confirmed by time studies (*8*). The large diffusion length of H in metallic Fe (~500 μm per 10 s) (*9*) may be the reason for the short relaxation time needed to achieve equilibrium.

Hydrogen dissolution into iron is significant at pressures ≥ 5 GPa (*10–12*). The product, FeH*x*, quickly decomposes into Fe and H_2 at ambient pressure, so the H concentration in FeH*x* is difficult to determine. In the case of crystalline FeH*x*, an in situ x-ray diffraction technique was used to determine the H concentration from the expansion of the unit cell volume of Fe lattice at high pressures, assuming a constant volume expansion per H atom (*6*). However, the x-ray diffraction method cannot be applied for molten FeH*x*.

In previous high-pressure melting experiments on FeH*x* (*4, 7*), H completely escaped from the Fe during decompression at a rate of several gigapascals per hour after the FeH*x* was synthesized (*13*). In these experiments, therefore, the pressure was released rapidly (1.5 GPa/s) to prevent H from escaping from the FeH*x*. As a consequence of such rapid decompression, numerous bubbles formed in the recovered Fe grains (Fig. 1). These bubbles are now empty but must have been filled with H_2 because no other volatile components were available in these experiments (*3*). Distribution of the bubbles differs in the solid and the molten FeH*x* phases. This difference can be explained by the different nucleation sites of H_2 available in each phase. Solid FeH*x* is quenched without any textural change. During decompression, the bubbles nucleate homogeneously in the Fe matrix. On the other hand, molten FeH*x* is quenched into an aggregate of quench crystals of solid FeH*x*. During decompression, the bubbles nucleate heterogeneously along the grain boundaries.

The volume fraction of the H_2 bubbles in the Fe was determined from the backscattered electron images of Fe grains recovered after the experiments (Fig. 2). If the H cannot escape from FeH*x* grains during quenching and decompression, then the H concentration in FeH*x* should be equal to the total volume of the bubbles multiplied by the density of H in the bubbles. The density of H in the bubbles soon after decompression was estimated by comparing a bubble volume in solid FeH*x* with a reported H concentration in crystalline FeH*x* measured in the in situ experiment (*6*). For this comparison, a series of rapid decompression experiments at 5.0 GPa were carried out, and a volume fraction of bubbles of 0.30 was obtained for solid FeH*x* just below the FeH*x* solidus. In the same Fe-MgO-SiO_2-H_2O system at 4.9 GPa and just below the FeH*x* solidus, an H/Fe molar ratio of 0.4 was determined from the lattice constants

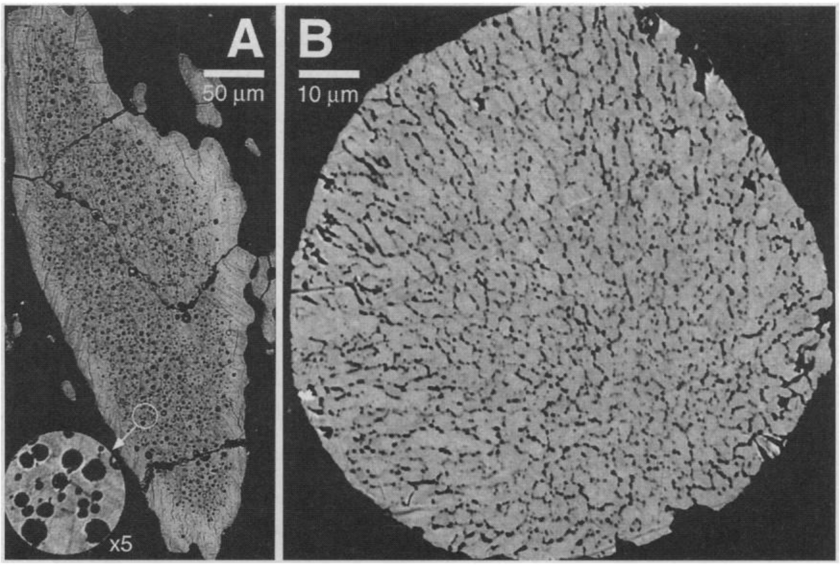

Fig. 1. Backscattered electron images of recovered Fe grains in a polished cross section at 1200°C. Bright areas are metallic Fe. Dark areas in the grains are H bubbles. (**A**) Bubbles formed after solid FeH*x* single crystal. Because of instant decompression, H became visible as numerous small bubbles. An enlarged image of the bubbles is shown on the same scale with those bubbles in molten FeH*x*. (**B**) Bubbles formed after molten FeH*x*. The H bubbles formed along the grain boundaries of the quench crystals. Both (A) and (B) showing different textures coexist in the same recovered charge of run 499.

Department of Earth and Planetary Sciences, Tokyo Institute of Technology, 2-12-1 Ookayama, Meguro-ku, Tokyo 152, Japan.

of solid FeH*x* (6). From these values, the density of H in the bubbles, when they reached their final size, was calculated as 0.13 g/cm^3. This density can be applied for the rapid decompression experiments at ≥5 GPa, because H bubble formation was not triggered until the pressure was released to <5 GPa even if the decompression started at a higher pressure (*10*, *11*). Therefore, I used this density of H to estimate the H concentration in solid and molten FeH*x* at 7.5 GPa (Fig. 2).

The H concentration in molten FeH*x* increases with increasing temperature, from ~0.4 at 1200°C to ~0.7 at 1500°C (Fig. 2). At 1200°C, solid and molten FeH*x* coexist, and the latter is enriched in H by 20 mole percent. This is consistent with thermodynamic calculation, which predicts a slightly higher H concentration in the melt than in the solid (5). The H distribution coefficient between molten and solid FeH*x* is

$$D^{\mathrm{H}}_{\mathrm{M/S}} = \frac{[\mathrm{H/Fe}]_{\mathrm{melt}}}{[\mathrm{H/Fe}]_{\mathrm{solid}}} = 1.2 \qquad (1)$$

To determine the metal-silicate melt partition coefficient of H, the composition of FeH*x* and coexisting silicate melt must be determined in each experiment. I estimated the silicate melt composition by mass-balance calculation (Table 1) and determined the compositions of the olivine and pyroxene in each recovered charge by electron microprobe analysis (3). The Fe^{2+}/Mg molar ratio of the quenched silicate melt was then calculated from the composition of residual olivine by using $K^{\mathrm{Mg\text{-}Fe}}_{\mathrm{melt\text{-}oliv}} = 0.36$ (*14*). For a totally molten system, it was assumed that most magnesian olivine in the quench crystals was in equilibrium with the melt at the beginning of quench crystal growth. Then the FeO/$MgSiO_3$ ratio of the bulk silicate (*n*) was determined from the relative volume fraction and composition of the coexisting phases. The $H_2O/MgSiO_3$ ratio of the bulk silicate should be $m - n$, where *m* is the starting $H_2O/MgSiO_3$ ratio, because all the FeO in the silicate was produced by compensation of an equivalent mole fraction of H_2O by reaction 2. This amount of H_2O should have been dissolved in the silicate melt.

From the composition of the coexisting FeH*x* (Fig. 2) and silicate melt (Table 1), the H partitioning coefficient in the MgO-SiO_2-Fe-O-H system at 7.5 GPa is determined as a function of temperature. Hydrogen is a univalent cation in silicate melt, whereas it is neutral in FeH*x* (*15*). Therefore, during FeH*x* formation in hydrous silicate melt, the H cation accepts one electron from the Fe atom. Thus, the reactions of H reduction and Fe oxidation are coupled:

$$\underset{\text{metal}}{\mathrm{Fe}} + \underset{\text{silicate melt}}{\mathrm{H_2O}} \rightleftharpoons \underset{\text{silicate melt}}{\mathrm{Fe}^{2+}} + \underset{\text{silicate melt}}{\mathrm{O}^{2-}} + \underset{\text{metal}}{2\mathrm{H}} \qquad (2)$$

The equilibrium constant *K* is determined from activities *a* of the products divided by the reactants:

$$K = \frac{a_{\mathrm{Fe}^{2+}}\, a_{\mathrm{O}^{2-}}\, a_{\mathrm{H}}{}^{2}}{a_{\mathrm{Fe}}\, a_{\mathrm{H_2O}}} \qquad (3)$$

The natural logarithm of *K* has a linear dependence on the reciprocal absolute temperature:

$$\ln K = -\frac{\Delta G^\circ}{RT} = -\frac{\Delta H^\circ}{RT} + \frac{\Delta S^\circ}{R} \qquad (4)$$

where ΔG° is change in Gibbs free energy, Δ*H*° is change in enthalpy, and Δ*S*° is change in entropy.

To calculate *K* from the experimental results, I assumed an activity model for each component in Eq. 3 (Table 2). These activities are defined as a simple mole fraction of the component to all available sites in the host phase except for a_{Fe}, which was analytically defined from a_{H} through the Gibbs–Duhem relation. To estimate the number of interstitial sites (Table 2), I assumed a close-packing structure for the molten Fe and the silicate melt. This is valid because the coordination number in a metal does not change much upon melting (5), and because, under the pressure adopted in this experiment, ultrabasic silicate melt is a little less dense than the silicate minerals of the oxygen close-packing structure (*16*). The $a_{\mathrm{O}^{2-}}$ and $a_{\mathrm{H_2O}}$ values may be slightly overestimated because OH^- may form from H_2O molecules and bridging oxygens in the silicate melt (*17*). Because there are not many bridging oxygens in the silicate melt with orthosilicate-like composition (Table 1) (*14*, *18*), this overestimation may not be large.

There was a linear correlation between ln *K* and the reciprocal absolute temperature (Fig. 3). From the slope of the regression line, I estimated the enthalpy change of reaction 2 as 140 ± 27 kJ/mol within 2σ (*19*). This large and positive change in

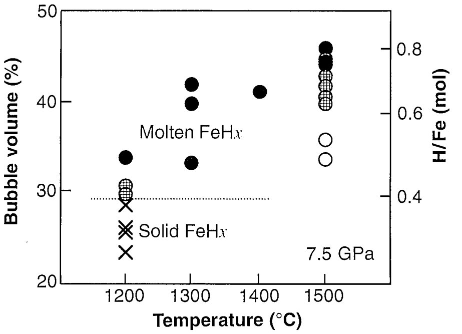

Fig. 2. Bubble fraction of recovered iron grains (left ordinate) and hydrogen concentration in FeH*x* (right ordinate) as a function of temperature (abscissa). By comparing the result of rapid decompression experiments with the in situ measurement (6), the H density in the bubbles is estimated as 0.13 g/cm^3. This density is used for estimating the H concentration in FeH*x*. Open circles, molten FeH*x* with starting H_2O concentration $m \leq 1.2$; hatched circles, molten FeH*x* with $1.2 < m \leq 1.4$; solid circles, molten FeH*x* with $1.4 < m$; crosses, solid FeH*x*.

Table 1. Run condition, starting composition, and recovered silicate composition of experiments; ? indicates unknown.

Run	*P* (GPa)	*T* (°C)	Time (s)	Starting composition $MgSiO_3$ *m* H_2O + Fe	Silicate bulk composition $MgSiO_3$·*n* FeO·(*m* − *n*) H_2O		Silicate melt composition			Silicate melt fraction (%)	No. of analyses		ln *K* (±1σ)
				m	*n*	*m* − *n*	Mg/Si	Fe/Si	H_2O/Si		Solid FeH*x*	Molten FeH*x*	
499	7.5	1200	300	1.40	?	?	0.83*	0.87*	1.03†	~20	4	2	−3.6 ± 0.1
504	7.5	1200	1200	1.60	0.70	0.90	0.96*	0.74*	1.03	90	0	1	−3.4
500	7.5	1300	300	1.60	0.77	0.83	1.00	0.77	0.83	99	0	3	−2.4 ± 0.6
508	7.5	1400	60	1.55	0.77	0.78	1.00	0.77	0.78	100	0	1	−2.0
603	7.5	1500	10	1.45	0.72	0.73	1.00	0.72	0.73	100	0	3	−1.4 ± 0.2
570	7.5	1500	15	1.25	0.70	0.55	1.00	0.70	0.55	100	0	5	−1.5 ± 0.3
514	7.5	1500	60	1.00	0.77	0.23	1.00	0.77	0.23	100	0	2	−1.5 ± 0.2

*A (Mg + Fe)/Si ratio of 1.7 is assumed (*18*). †The same ratio is used with run 504.

enthalpy indicates that H partitioning into molten FeH*x* increases with increasing temperature. The correlation enables *K* to be extrapolated to temperatures higher than the experimental conditions, which are relevant to the H partitioning into molten iron during Earth's core formation.

Ringwood (*20*) proposed a two-component model for an averaged composition of the Earth-forming material, based on the abundance of lithophile elements in the mantle, and the condensation temperature of elements from a gas of solar composition (*21*). Using his model, I assumed that Earth was formed from 90 weight % of a high-temperature component, such as enstatite chondrites minus volatiles, and 10 weight % of a low-temperature component, such as CI chondrites. This corresponds to 65% enstatite, 33% metallic Fe, and 2% H_2O if minor elements are neglected (*22*). Starting with this composition, I calculated the H distribution between silicate melt and molten iron at temperatures up to 2000°C at 7.5 GPa by using the regression line of the equilibrium constant (Fig. 3). At temperatures above the dry silicate solidus (~1800°C) (*23*), a_{H_2O} decreases as reaction 2 proceeds to the right, and finally equilibrium is achieved when more than 95 mol% of H_2O is consumed to form FeH*x*. On the other hand, at temperatures below the dry silicate solidus, the silicate melt solidifies as the H_2O is consumed to form FeH*x*. Because the H_2O concentration in the silicate melt is fixed at a given pressure and temperature when the melt coexists with solid silicate phases (*18*), a_{H_2O} does not decrease but is kept constant even if reaction 2 proceeds to the right. Then the silicate melt fraction decreases, and eventually all the H goes into FeH*x*. In other words, the iron-water reaction in primordial Earth dries the system out, so that wet melting of the silicate is prohibited below the dry silicate solidus.

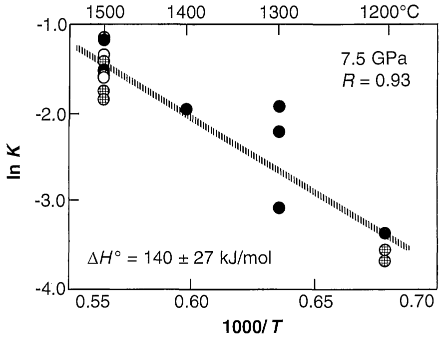

Fig. 3. Equilibrium constant of the H partitioning reaction 2 plotted against reciprocal absolute temperature. Equilibrium constant increases with temperature, so the reaction is endothermic. The enthalpy change of the reaction is estimated from the slope of the regression line (see Eq. 4). Symbols are the same as in Fig. 2.

The metal-silicate melt partitioning of H in primordial Earth presumably occurred at the bottom of the magma ocean, where molten metal may have stagnated as iron ponds (*24*). Most of the H_2O accreted to Earth should have dissolved into the magma ocean, whereas an impact-induced steam atmosphere in equilibrium with the magma ocean may have held H_2O in a mass equivalent to the present oceans (*25*). Therefore, if the pressure at the bottom of the magma ocean was ≥7.5 GPa, more than 95% of H_2O accreted to Earth should have reacted with Fe to form FeH*x*. Then the iron ponds sank to the core by large-scale gravitational instability (*24*), during which time the pressure and temperature adjacent to the molten iron increased. Because the volume change of reaction 2 is negative (*10, 26, 27*) with a positive change in enthalpy, *K* should increase with increasing pressure and temperature. Therefore, once H is partitioned into the molten iron at the bottom of the magma ocean, it never returns to the silicate and should have gone into the core.

Table 2. Activity models for components in Eq. 3. These are defined as a mole fraction of the component to all available sites in each phase except for a_{Fe}.

Phase	Component	No. of close-packing sites	No. of interstitial sites*	Activity	References
Molten iron	Fe	N_{Fe}		$\left(1-\frac{N_H}{3N_{Fe}}\right)^3$	This study by Gibbs–Duhem relation
	H		$N_{Fe} \times (2^{IV} + 1^{VI})$	$\frac{N_H}{3N_{Fe} - N_H}$	(*5, 26*)
Silicate melt	O^{2-}	$N_{O^{2-}} + N_{H_2O}$		$\frac{N_{O^{2-}}}{N_{O^{2-}} + N_{H_2O}}$	(*17*)
	H_2O	$N_{O^{2-}} + N_{H_2O}$		$\frac{N_{H_2O}}{N_{O^{2-}} + N_{H_2O}}$	(*17*)
	Fe^{2+}		$(N_{O^{2-}} + N_{H_2O}) \times 1^{VI}$	$\frac{N_{Fe^{2+}}}{N_{O^{2-}} + N_{H_2O}}$	This study

*Roman numerals show coordination number of each interstitial site.

Hydrogen abundance in the core has been discussed by many authors (*4, 6, 10, 11, 13, 22, 26, 28*). If the two-component model (*20*) is valid for the amount of volatile components, including S, C, and H_2O, and if nearly 100% of the H_2O has reacted with Fe to form FeH*x*, then the molar concentration of H in the core becomes H/Fe = 0.41, which exceeds an S/Fe ratio of 0.03 and a C/Fe ratio of 0.05 (*22*). Then the density of molten Fe in the outer core is reduced by H by 5.5%, which also exceeds the contribution of S (1.1%) and C (2.2 to 2.7%) (*26*). The expected density reduction of ~9% by H, S, and C agrees with the observed density deficit of the outer core, so that further density reduction by dissolution of O is not necessary (*20*). Hydrogen may be the primary light element in the core. This is true not only for the molten outer core but also for the solid inner core, because Eq. 1 indicates that the H/Fe ratio in the inner core may reach 0.34 ($0.41/D^{H}_{M/S}$). This amount of H reconciles about two-thirds of the observed inner core density deficit of ~7% (*26*).

REFERENCES AND NOTES

1. E. Takahashi, T. Shimazaki, Y. Tsuzaki, H. Yoshida, *Phil. Trans. R. Soc. London A. Math. Phys. Sci.* **342**, 105 (1993).
2. During these experiments, the iron-water reaction (Eq. 2) buffers p_{H_2} in the capsule as long as H_2O is dissolving in the silicate melt, despite H_2 continuously escaping through the capsule wall. After all the H_2O sealed in the capsule is exhausted, the p_{H_2} is no longer buffered but decreases with time. To evaluate the minimum amount of H_2O needed to maintain p_{H_2} throughout the experiments, the equilibrium constant, *K* in Eq. 3, at 1500°C was determined with various amounts of H_2O in the starting material, with an $H_2O/MgSiO_3$ molar ratio (*m*) ranging from 0.23 to 1.45. The results showed that *K* increases with increasing H_2O concentration until *m* reaches 1.0. However, when *m* exceeds 1.0, *K* becomes constant even if the H_2O concentration increases. Therefore, $m = 1.0$ is the minimum amount of H_2O needed to keep p_{H_2} at 1500°C in the large (7 mm by 5 mm) capsules. At lower temperatures H_2 is expected to escape more slowly from the capsules, and the equilibrium should be maintained for a longer duration, so the minimum amount of H_2O at 1500°C should be valid at lower temperatures. The experiments satisfying $m \geq 1.0$ were selected for this study (Table 1). For synthesis of molten FeH*x* under the equilibrium condition, the large capsules in this study are essential but not adequate when there is insufficient H_2O.
3. T. Okuchi and E. Takahashi, in *High Pressure-Temperature Research: Properties of Earth and Planetary Materials*, M. H. Manghnani and Y. Syono, Eds. (American Geophysical Union, Washington, DC, in press).
4. T. Suzuki, S. Akimoto, Y. Fukai, *Phys. Earth Planet. Inter.* **36**, 135 (1984).
5. Y. Fukai, *J. Less-Common Metals* **8**, 172 (1991).

6. T. Yagi and T. Hishinuma, *Geophys. Res. Lett.* **22**, 1933 (1995).
7. T. Hishinuma, T. Yagi, T. Uchida, *Proc. Jpn. Acad.* **70B**, 71 (1994).
8. The settling time of the droplets depends on the viscosity of the silicate melt. For the experiment of long duration at high temperature, the amount of H_2O in the starting material should be reduced to make the settling time longer to prevent interaction between the droplets and the capsule wall. In the experiments with various amounts of H_2O in the capsule, comparison of the H concentration in FeHx measured in this study is less meaningful to confirm the equilibrium because it depends on a_{H_2O} in the silicate melt. Comparison of the equilibrium constant *K* rather than the H concentration in FeHx is more suitable to confirm the equilibrium of reaction 2. The value of *K* at 1200°C and at 1500°C shows little variation despite various run durations (Table 1).
9. Y. Fukai and H. Sugimoto, *Adv. Physics* **34**, 263 (1985).
10. Y. Fukai, *Nature* **308**, 174 (1984).
11. J. V. Badding, R. J. Hemley, H. K. Mao, *Science* **253**, 421 (1991).
12. M. Yamakata, T. Yagi, W. Utsumi, Y. Fukai, *Proc. Jpn. Acad.* **68B**, 172 (1992).
13. Y. Fukai and S. Akimoto, *ibid.* **59B**, 158 (1983).
14. T. Inoue and H. Sawamoto, in *High-Pressure Research: Application to Earth and Planetary Sciences*, Y. Syono and M. H. Manghnani, Eds. (Terra Scientific Publishing Company/American Geophysical Union, Tokyo/Washington, DC, 1992), pp. 323–331. The $K^{\text{Mg-Fe}}_{\text{melt-oliv}}$ was calculated from the composition of the coexisting olivine and hydrous silicate melt reported here.
15. Y. Fukai, *Jpn. J. Appl. Phys.* **22**, 207 (1983).
16. A. Suzuki, E. Ohtani, T. Kato, *Science* **269**, 216 (1995).
17. E. Stolper, *Geochim. Cosmochim. Acta* **46**, 2609 (1982).
18. T. Inoue, *Phys. Earth Planet. Inter.* **85**, 237 (1994).
19. Reaction 2 can be rewritten with the FeO component in an ideal solution of oxides instead of Fe^{2+} and O^{2-} in the silicate melt. This approach yields $\Delta H° = 136 \pm 27$ kJ/mol, which is almost identical to the value reported here.
20. A. E. Ringwood, *Geochem. J.* **11**, 111 (1977).
21. L. Grossman and J. W. Larimer, *Rev. Geophys. Space Phys.* **12**, 71 (1974).
22. Y. Fukai and T. Suzuki, *J. Geophys. Res.* **91**, 9222 (1986). In this paper, a detailed mass-balance calculation for estimating the core composition was done with the two-component model (*20*) for Earth's bulk inventory of the light elements.
23. E. Takahashi, *J. Geophys. Res.* **91**, 9367 (1986).
24. D. J. Stevenson, in *Origin of the Earth*, H. E. Newsom and J. H. Jones, Eds. (Oxford Univ. Press, New York, 1990), pp. 231–249.
25. Y. Abe and T. Matsui, *J. Geophys. Res.* **90**, C545 (1985); *ibid.* **91**, E291 (1986).
26. Y. Fukai, in *High-Pressure Research: Application to Earth and Planetary Sciences*, Y. Syono and M. H. Manghnani, Eds. (Terra Scientific Publishing Company/American Geophysical Union, Tokyo/Washington, DC, 1992), pp. 373–385.
27. ———, *Kagaku* **54**, 36 (1984) (in Japanese).
28. D. J. Stevenson, *Nature* **268**, 130 (1977); *Science* **214**, 611 (1981).
29. The author thanks E. Takahashi for discussion and criticism, for reading and correcting this report, and for help and advice in the high-pressure experiments. Critical reviews by two anonymous referees improved this manuscript very much. Supported by the Foundation for Research Fellowships of Japan Society for the Promotion of Science for Young Scientists (DC1). Contribution 17 from the Magma Factory.

21 April 1997; accepted 20 October 1997

Correlations Between Ground and Excited State Spectra of a Quantum Dot

D. R. Stewart, D. Sprinzak, C. M. Marcus,* C. I. Duruöz, J. S. Harris Jr.

The ground and excited state spectra of a semiconductor quantum dot with successive electron occupancy were studied with linear and nonlinear magnetoconductance measurements. A direct correlation was observed between the *m*th excited state of the *N*-electron system and the ground state of the ($N + m$)-electron system for *m* up to 4. The results are consistent with a single-particle picture in which a fixed spectrum of energy levels is successively filled, except for a notable absence of spin degeneracy. Further departures from the single-particle picture due to electron-electron interaction were also observed. Magnetoconductance fluctuations of ground states show anticrossings where wave function characteristics are exchanged between adjacent levels.

Quantum dots (QDs) are small electrically conducting regions, typically 1 μm or less in size, containing from one to a few thousand electrons (*1*). Because of the small volume, the allowed electron energies within the dot are quantized, forming a discrete spectrum of quantum states, not unlike the energy levels of an atom. However, in contrast to the ordered shell structure of atomic spectra—a consequence of the spherically symmetric potential that binds the electrons—the generic energy spectrum of a QD (lacking any special symmetry) shows no shell structure, but instead has universal statistical properties associated with the underlying universality of quantum chaos (*2*).

Disordered or irregularly shaped QDs are examples of so-called mesoscopic systems—small electronic structures intermediate in size between atoms and macroscopic (classical) objects that have universal spectral and transport properties that are independent of material, shape, or disorder. In the past few years, a remarkable set of connections between mesoscopic systems, complex quantum systems such as heavy nuclei (where the statistical approach to spectra was first developed), quantum systems whose classical analogs are chaotic, and random matrix theory has emerged, providing deep theoretical insight into the generic properties of quantum systems (*2*). These connections are based principally on noninteracting, single-particle spectral properties; only recently has attention been focused on mesoscopic systems in which interactions between particles and quantum interference play equally important roles. It is in this context that the generic spectral features of multi-electron QDs are of great interest.

The electronic spectra of QDs are governed by the interplay of two energy scales: the Coulomb interaction or charging energy associated with adding a single electron to the dot, and the confinement energy associated with quantization due to the confining potential. In lateral semiconductor QDs the charging energy is typically an order of magnitude larger than the quantum confinement energy, which suggests that the quantum spectrum of the ($N + 1$)-electron QD may be uncorrelated with the spectrum of the *N*-electron QD (*1*). On the other hand, in recent theoretical work (*3*) it has been argued that modifications to the universal single-particle spectrum resulting from electron-electron interactions should be smaller than, or at most comparable with, the typical energy spacing between quantum levels, suggesting that spectra for successive *N* may remain correlated.

Previous investigation of QD spectra by transport and capacitance spectroscopy has concentrated on analysis of the "addition" energy spectrum composed of the ground states of the QD for successive numbers of electrons (*1*, *4*–*6*). Several experiments (*7*–*10*) have also probed the "excitation" spectrum of quantum levels in the QD for fixed electron numbers using nonlinear conductance measurements. These measurements showed spectral features attributed to electron-electron interactions such as spin blockade (9) and clusters of resonances identified with a single excited state (*10*). Many-body calculations for few-electron systems ($N \leq 5$) have explained some of the experimentally observed features in terms of spin and spatial selection rules (*11*), spectrally dominant center-of-mass excitation modes

---

D. R. Stewart, Department of Applied Physics, Stanford University, Stanford, CA 94305, USA.
D. Sprinzak, Department of Physics, Stanford University, Stanford, CA 94305, USA, and Braun Center for Submicron Research, Department of Condensed Matter Physics, Weizmann Institute of Science, Rehovot 76100, Israel.
C. M. Marcus, Department of Physics, Stanford University, Stanford, CA 94305, USA.
C. I. Duruöz and J. S. Harris Jr., Department of Electrical Engineering, Stanford University, Stanford, CA 94305, USA.

*To whom correspondence should be addressed.